

In-Flight Mixed Phase Ice Accretion Prediction on Finite Wings with TAICE-3D

Erdem Ayan and Serkan Özgen†*

**Turkish Aerospace Industries, Aerodynamics, Modeling and Control Department
Kazan 06980 Ankara, Turkey*

*†Middle East Technical University, Aerospace Engineering Department,
Çankaya 06531 Ankara, Turkey*

eayan@tai.com.tr · sozgen@ae.metu.edu.tr

Abstract

Mixed phase ice accretion prediction capability of the 3D version of TAICE is presented in this study. First, computational approach while performing numerical analyses is detailed. In this part, the effect of the number of panels used in the chordwise direction and the effect of number of time steps used in the multi-step analyses are discussed. Then, in-flight ice formation results on finite wings are given. COX and TUBS experimental results are used for ice shape comparisons on wing sections in order to validate the tool. Thus, the present study is an effort to extend the previous work on two-dimensional analysis to three dimensions and to predict ice shapes with the new tool.

NOMENCLATURE

AOA	Angle of Attack
c	Chord
CS	Certification Specification
EASA	European Aviation Safety Agency
FAA	Federal Aviation Administration
HAIC	High Altitude Ice Crystals
IWC	Ice Water Content
LWC	Liquid Water Content
MMD	Mean Mass Diameter
MVD	Mean Volumetric Diameter
NASA	National Aeronautics and Space Administration
NRC	National Research Council Canada
RH	Relative humidity
t	Time
T	Temperature
T_s	Static Temperature
T_t	Total Temperature
V	Velocity magnitude of cloud particle with respect to the flow field
V_∞	freestream velocity
ρ	Density

1. Introduction

For a long time and until very recently, icing conditions and related requirements were covered by certification specifications, which only take into account ice accretion due to water droplets. Specified clouds in CS Appendix C include only liquid water content and corresponding droplet sizes are smaller than 50 microns. However, following the review of icing related events, it was realized that they had occurred in icing conditions that were not addressed by Appendix C. Some power loss events have been noted in the last two decades at high altitudes in convective weather conditions where ice crystals exist as well. Moreover, some of these events involved multi-engine power losses. Although the

MIXED PHASE ICING WITH TAICE-3D

events did not result in accidents, they were considered as serious safety threats. Therefore, it was proposed to amend CS-25 and FAR-25 to better protect large airplanes certified for flight in icing conditions.² Thus, both FAA⁴ and EASA³ have extended the icing envelopes to include Supercooled Large Droplets and Mixed Phase Clouds in Appendix O and Appendix P (Appendix D in FAR-25), respectively.

Ice crystals are formed generally within the tropical clouds and may have various shapes. They differ from liquid droplets in terms of their shape and they do not have to be exactly spherical. Thus, for accurate prediction of the trajectories, drag force coefficient, heat transfer and phase change models should be modified for non-spherical particles in order to be used for ice crystals. For drag coefficient calculations Hölzer-Sommerfeld model is selected within the drag coefficient models which are applicable to non-spherical particles.¹² Moreover, NASA relation which was originally developed by Wright *et al.*,¹⁶ is used for erosion prediction with the further calibrated data as given in another study of the authors.⁶ For impingement, heat transfer and phase change models, the relations, which are suggested by Trontin *et al.* are utilized in this study.¹⁵ Detailed information about the implemented models to TAICE is given in the authors' previous studies.⁶⁻⁸ Furthermore, modified Extended Messinger model is used for the prediction of ice shapes. Extended Messinger Model was originally developed by Myers.¹³ Instead of predicting the equilibrium temperature as in the Original Messinger Model, temperature variation is modeled within the ice and water layers to improve the accuracy of the predictions in his model. However, his model is applicable only to water droplet included problems. Thus, this model has been further extended by the authors to be used for mixed phase icing problems.⁶

2. Computational Approach

Computational analysis begins with the calculation of the flow field variables as in the 2-D version. 3-D panel method is used to calculate the velocity distribution around the given geometry. Liquid and solid cloud particles are released at the same time at a sufficiently far upstream location and the Lagrangian method is used to compute the trajectories. Since trajectory calculations constitute nearly 99% of the whole computational time, this part is parallelized by using MPI. The given geometry is divided into spanwise panels and trajectories of the cloud particles which are released for each spanwise panel are computed with different threads.¹⁴ Four spanwise panels are used in this comparison study. For the thermodynamic relations, two dimensional Integral Boundary Layer relations are utilized. Then, collection efficiencies are computed at each chordwise panel upon calculating impact locations of the particles. Finally, ice accretion predictions are performed by using the modified version of the Extended Messinger Model as discussed in the introduction part and ice shapes are obtained.

The developed tool allows performing multi-layer analyses and in order to increase the accuracy, total exposure time is divided into segments. Since accreted ice affects the flow field variables, whole analysis is repeated for each time segment in the multi-layer mode. To show the trajectories COX-10 experimental case is analyzed.⁵ Constant chord is assumed along the wing having 2.74 m span, which is the wind tunnel test section width as indicated in the study of Al-Khalil *et al.*⁵ Parameters are given in Table 1 for this run condition.

Table 1: COX-10 run condition⁵

Case	Airspeed (m/s)	Total Temp. (°C)	Total Press. (kPa)	IWC (g/m ³)	LWC (g/m ³)	Crystal MVD (μm)	Droplet MVD (μm)
10	53.60	-5.55	100	0.7	0.7	200	20

Droplet and ice crystal particle trajectories are calculated for case #10 and shown in Figure 1. Moreover, a closer view is also included for both type of particles as indicated in Figure 2.

In this sample case, the total wing span is divided into 4 segments and particle trajectories are calculated in the middle of each section. Since the twist angle of the wing is zero and has constant chord, each segment of the wing sees the same angle of attack in this validation case. Then, accreted ice shapes of each segment are connected with the neighboring ones to obtain the 3-D ice shape.

Since crystals have greater MVD, their impingement zone is wider on the wing. Thus, the difference between upper and lower release point Z coordinates are higher and step size of the crystals is increased in order to reduce computational time. Moreover, as it is depicted in the closer view in Figure 2, droplets deviate more than crystals when they come closer to the wing due to their smaller size.

Collection efficiency distributions are shown in Figure 3 for both type of particles. As discussed before, ice crystals impact at a wider zone and the highest value of the collection efficiency is higher when compared with water droplets.

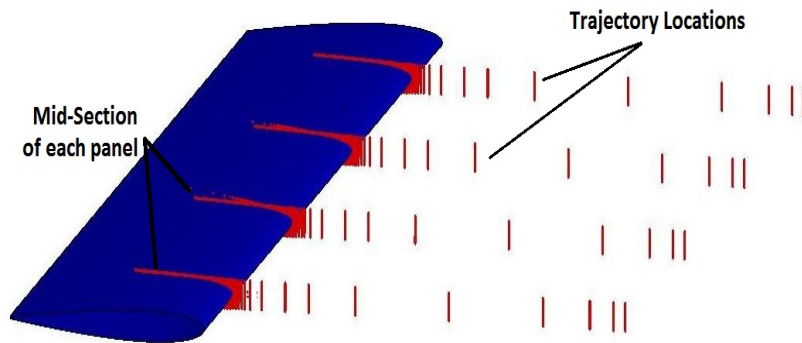


Figure 1: Crystal trajectories at $V_\infty = 53.60$ m/s, $T_t = -5.55$ °C, $MVD = 200$ μm .

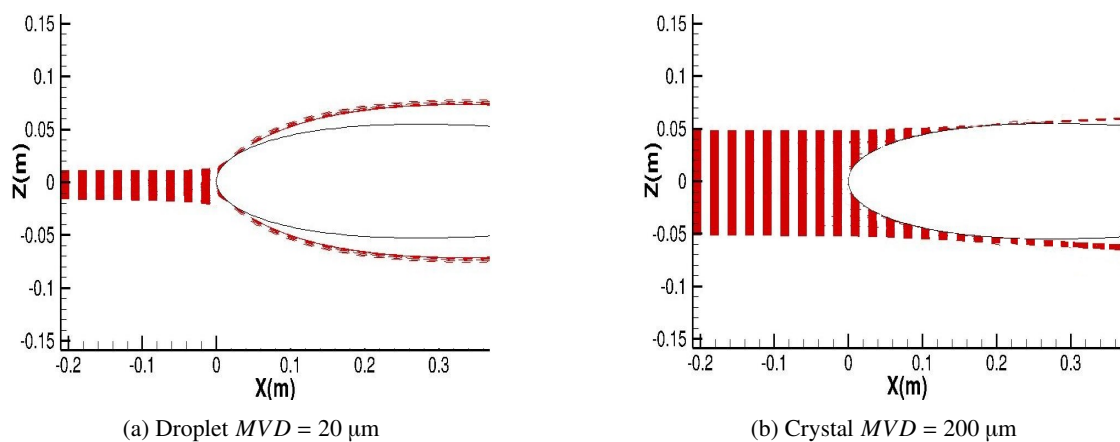


Figure 2: Particle trajectories closer view at $V_\infty = 53.60$ m/s, $T_t = -5.55$ °C. (a) Droplets (b) Crystals

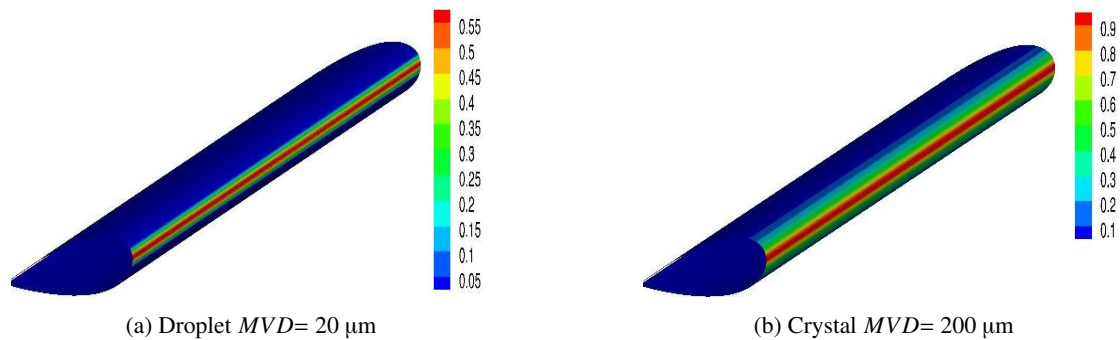


Figure 3: Collection efficiency comparison of particles at $V_\infty = 53.60$ m/s, $T_t = -5.55$ °C. (a) Droplets (b) Crystals

3. Assessment of Parameters Affecting Ice Shapes

This section gives information about the analysis parameters which affect the accreted ice shapes. Analyses are performed by varying each parameter and results are compared with glaze icing experimental case # 10 as given in Table 1.⁵

3.1 Number of Time Steps

It is known that accreted ice on body has influence on the flowfield. Single step analyses mostly lead to wrong ice shapes due to this reason. Moreover, too much increase in the number of time steps is also not preferred due to possible numerical errors such as round off. Thus, multi-step analyses should be performed in order to increase the accuracy of the predictions. Determining the number of time steps for each ice accretion analysis requires a preliminary work as stated in the LEWICE manual.¹ A relation similar to the recommended one in LEWICE manual is used in this study.

MIXED PHASE ICING WITH TAICE-3D

It should be noted that in order to use this relation for mixed phase icing cases, IWC is also included in addition to the LWC. However, this relation is applicable only to glaze ice conditions. Since in rime ice conditions, effect of ice crystals on accreted ice shapes can be negligible in most cases, including IWC in this relation may lead to wrong time step numbers.

$$TimeSteps = \frac{(LWC + IWC)(V)(t)}{(c)(\rho)0.01} \quad (1)$$

Analyses are performed for 1, 4, 6 and 10 steps and results are depicted in Figure 4. Required number of time steps is 6 according to equation 1 when nearest integer number is chosen. As expected, further increase in time step number does not increase the accuracy of the predictions. Moreover, since number of steps is directly related with the analyses duration, it causes further increase in the cost of the analyses. On the other hand, lower step analyses are also eliminated due to low accuracy.

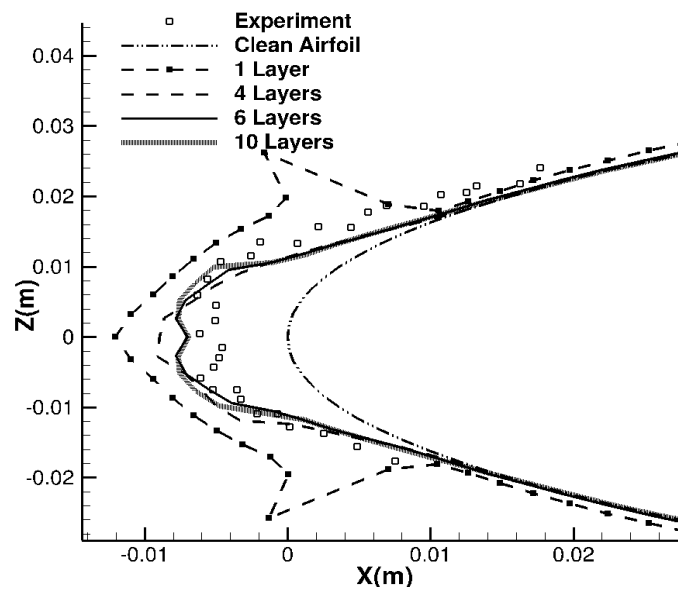


Figure 4: Ice shape comparisons for varying time step numbers from 1 to 10.

3.2 Number of Panels

Number of panels and boundary layer grids have direct influence on accreted ice on the surface. One reason is that they affect flowfield variables and heat transfer coefficients. Another reason is that the ice thicknesses are calculated for these points. A comparison is shown in Figure 5 for three different panel numbers and corresponding computational times are given in Table 2.

Table 2: Number of panels and boundary layer grids.

Case	Number of Panels	Number of Boundary Layer Grids	Computational Time per Layer (hr)
Coarse	101	401	0.5
Medium	401	801	0.9
Fine	701	1401	1.9

As it is depicted in Figure 5, varying number of panels changes the accreted ice shape on the surface. The accuracy of the coarsest one is good but capturing complicated ice shapes will be difficult due to less number of panels. Predictions of the finest one is also acceptable but it increases the computational time as shown in Table 2. Thus, having nearly the same accuracy, the medium one is chosen as the optimum number of panels and used in this study.

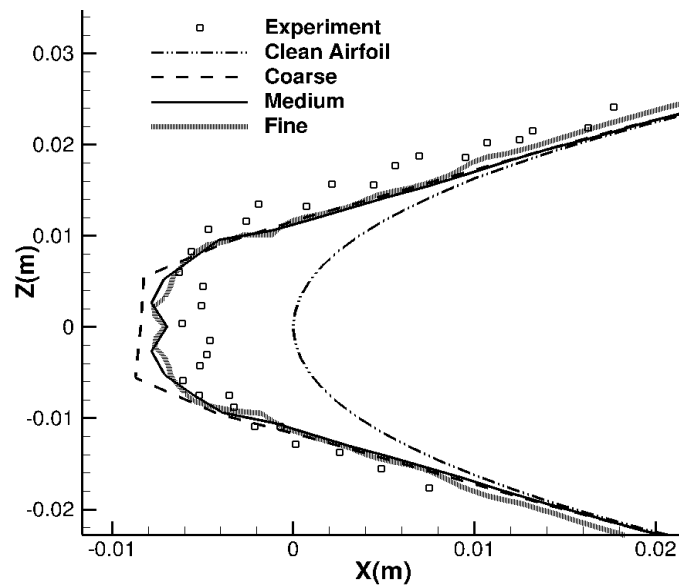


Figure 5: Ice shape comparisons for varying panel numbers.

4. Ice Shape Comparisons

4.1 Comparisons by Using COX Experimental Data

Al-Khalil *et al*⁵ performed mixed phase ice accretion experiments by using NACA-0012 airfoil having 0.9144 m chord length. The test section in the icing wind tunnel has a height of 1.83 m and a width of 2.74 m. Information related to calibrated impingement and erosion models can be found in the 2-D validation study.⁶ Ice accretion prediction runs are performed in 6 time steps which are calculated as the optimum time step number as discussed in the previous section. Medium dense panels are preferred in 3-D computations after compromising accuracy and required computational time. Span is divided into 4 segments and 301 panel points are used at each segment. For validation purposes, 2 rime ice and 2 glaze ice test cases are selected. Corresponding icing and flow parameters are introduced in Table 3.

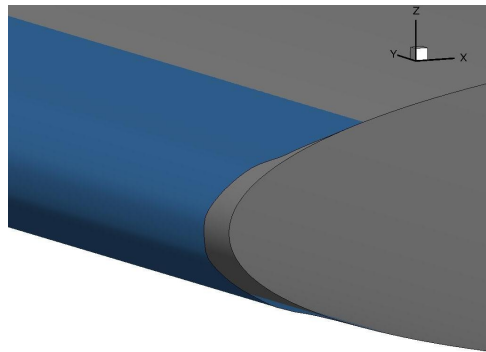
Table 3: Analyses conditions from COX experiments.⁵

Case	Airspeed (m/s)	Total Temp. (°C)	Total Press. (kPa)	IWC (g/m ³)	LWC (g/m ³)	Crystal MVD (μm)	Droplet MVD (μm)
9	53.60	-5.55	100	-	0.7	-	20
10	53.60	-5.55	100	0.7	0.7	200	20
19	53.60	-11.10	100	0.7	0.3	150	20
20	53.60	-11.10	100	0.3	0.7	150	20

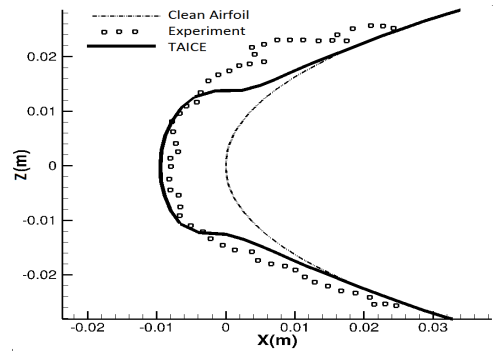
Computational and experimental ice shape comparison is given in Figure 6 for case #9 which is a pure droplet case. The computational result is consistent for this pure droplet case when compared with the experimental one.

Case #10 corresponds to another glaze ice condition. In this case, in addition to the droplets ice crystals having IWC equal to 0.7 g/m³ are included in the computations. Figure 7 indicates that including ice crystals in the analyses does not cause an increase in the accreted ice on the surface due to erosion.

MIXED PHASE ICING WITH TAICE-3D

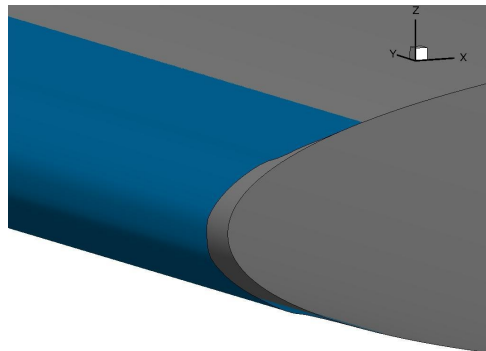


(a) Far view of the accreted ice.

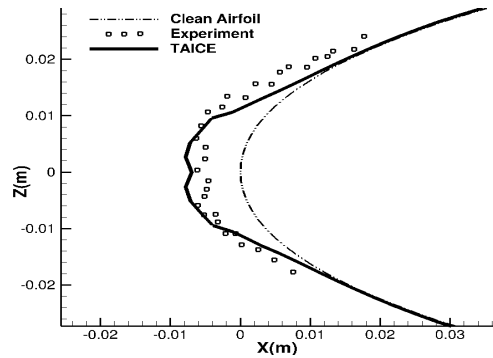


(b) Near view of the accreted ice and comparison with experimental data.

Figure 6: Accreted ice shape comparison for case #9, $T_t = -5.55\text{ }^\circ\text{C}$, $LWC = 0.7\text{ g/m}^3$. Black line shows accreted ice after 600 s.



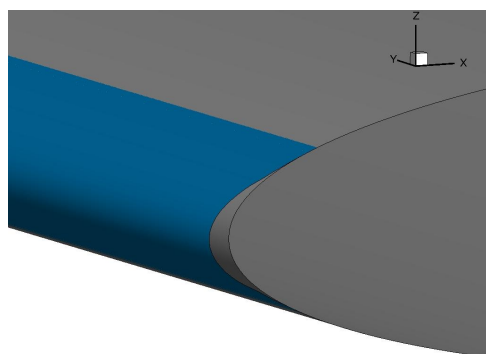
(a) Far view of the accreted ice.



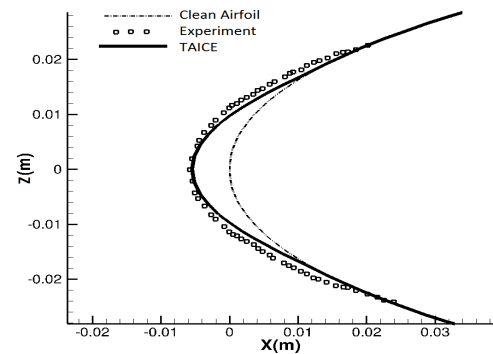
(b) Near view of the accreted ice and comparison with experimental data.

Figure 7: Accreted ice shape comparison for case #10, $T_t = -5.55\text{ }^\circ\text{C}$, $LWC = 0.7\text{ g/m}^3$, $IWC = 0.7\text{ g/m}^3$. Black line shows accreted ice after 600 s.

Case #19 and Case #20 correspond to rime ice conditions due to lower temperature. Ice crystals do not stick to surface in these cases and their contribution to ice shapes is only due to erosion. Corresponding ice shapes are shown in Figures 8 and 9 respectively.

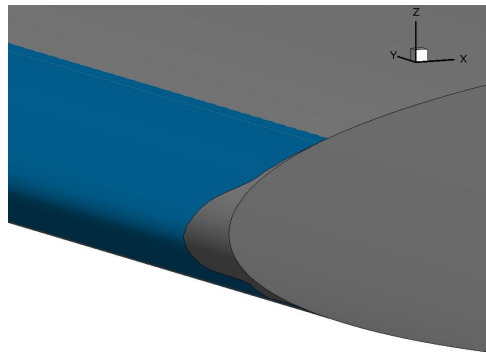


(a) Far view of the accreted ice.

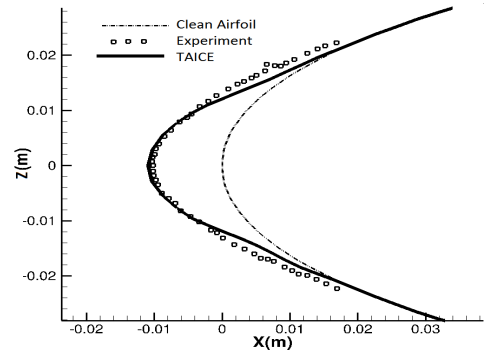


(b) Near view of the accreted ice and comparison with experimental data.

Figure 8: Accreted ice shape comparison for case #19, $T_t = -11.10\text{ }^\circ\text{C}$, $LWC = 0.3\text{ g/m}^3$, $IWC = 0.7\text{ g/m}^3$. Black line shows accreted ice after 600 s.



(a) Far view of the accreted ice.



(b) Near view of the accreted ice and comparison with experimental data.

Figure 9: Accreted ice shape comparison for case #20, $T_i = -11.10\text{ }^\circ\text{C}$, $LWC = 0.7\text{ g/m}^3$, $IWC = 0.3\text{ g/m}^3$. Black line shows accreted ice after 600 s.

4.2 Comparisons by Using TUBS Experimental Data

Icing experiments have been performed in the TUBS icing wind tunnel facility. NACA 0012 airfoil having 0.5 m chord has been used in these tests. Selected icing conditions for the validation analyses are given in Table 4.^{9,11} Tests have been performed at three different temperatures and at each temperature LWC and IWC values are varied. Droplet clouds are generated by a spray bar within 1.3 to 5 g/m^3 . On the other hand, ice crystals have a wider range and IWC of the injected crystals have been increased up to 13.6 g/m^3 . The accretion time is 2 minutes for all runs. Further details about the experiments and corresponding data can be found in the study of Baumert *et al* and Bansmer *et al*.⁹⁻¹¹

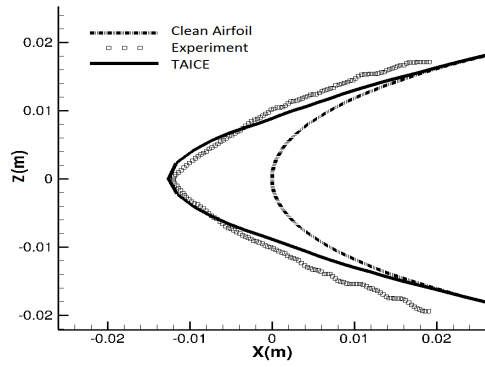
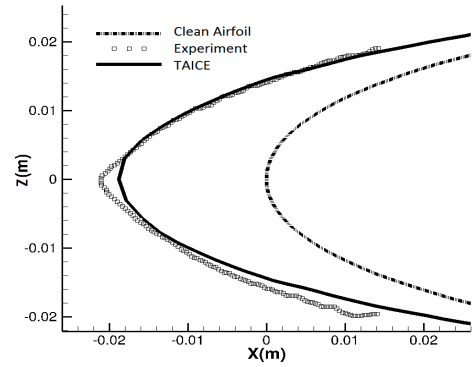
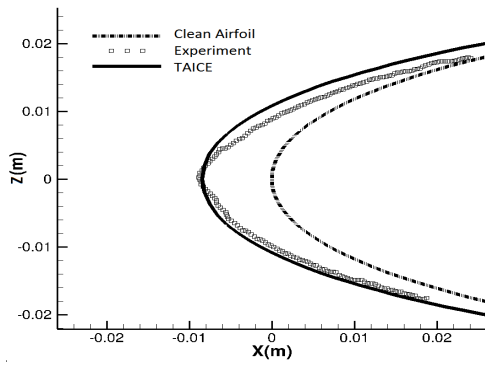
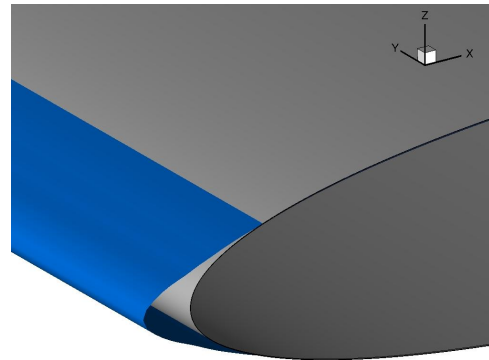
Table 4: Analyses conditions from TUBS experiments.

Case	Airspeed (m/s)	Static Temp. ($^\circ\text{C}$)	Static Press. (Pa)	IWC (g/m^3)	LWC (g/m^3)	AOA ($^\circ$)	RH (%)	Crystal MVD (μm)	Droplet MVD (μm)
1	40	0	101325	10.6	1.45	0	100	130	80
3	40	0	101325	8.7	3.4	0	100	130	80
5	40	0	101325	3.8	3.4	0	100	130	80
8	40	-5	101325	10.6	1.45	0	100	130	80
10	40	-5	101325	8.7	3.4	0	100	130	80
12	40	-5	101325	3.8	3.4	0	100	130	80
15	40	-15	101325	10.6	1.45	0	100	130	80
16	40	-15	101325	8.7	3.4	0	100	130	80

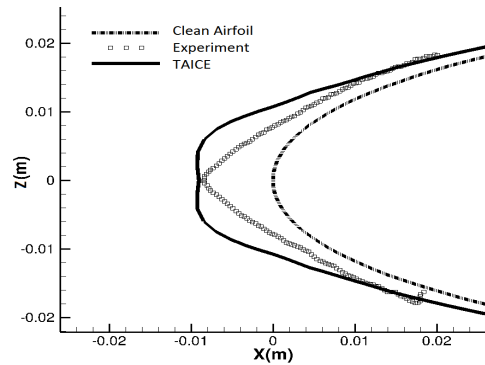
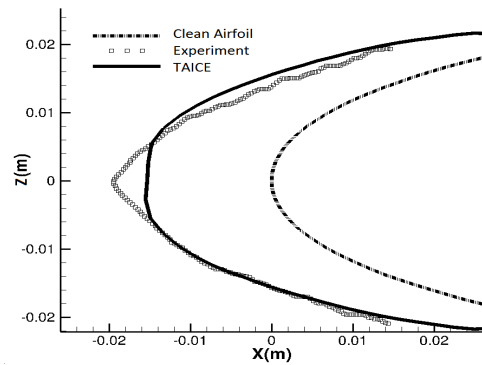
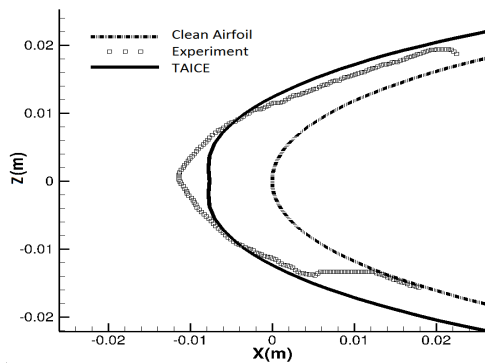
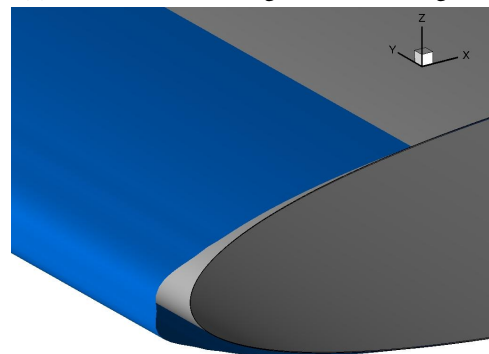
Accreted ice shapes on the NACA 0012 airfoil are depicted in Figures 10 - 12. In these figures, TAICE results are compared with the experimental data. Dotted lines refer to the experimental results and black lines correspond to the TAICE results. Differing from the COX experiments, IWC and LWC reach higher values here. Thus, erosion and impingement models require further calibration. Further information about the calibration parameters can be found in the referenced study of the authors.⁶

Following figures indicate that increasing the droplet ratio first causes more ice crystals to stick to the surface. However, further increase in the droplet ratio does not cause additional increase in the thickness of the accreted ice. On the contrary, reduction in the accumulated ice has been noted due to the erosion effect in these experimental tests. Analysis results seem consistent with the experimental data for all compared conditions. However, a few points should be emphasized here. First of all, accreted ice in the experiments have triangular shapes and sharp edges. On the other hand, ice shapes obtained with TAICE are more smooth. Moreover, at $-15\text{ }^\circ\text{C}$, TAICE overestimates the ice shapes, which indicates that the erosion effect is more than predicted at this temperature.

MIXED PHASE ICING WITH TAICE-3D

(a) Case #1, $IWC = 10.6 \text{ g/m}^3$, $LWC = 1.45 \text{ g/m}^3$ (b) Case #3, $IWC = 8.7 \text{ g/m}^3$, $LWC = 3.4 \text{ g/m}^3$ (c) Case #5, $IWC = 3.8 \text{ g/m}^3$, $LWC = 3.4 \text{ g/m}^3$ 

(d) Far view of the Case #1 accreted ice shape predicted by TAICE.

Figure 10: Accreted ice shape comparison at $T_s = 0^\circ\text{C}$. Black line shows accreted ice after 120 s.(a) Case #8, $IWC = 10.6 \text{ g/m}^3$, $LWC = 1.45 \text{ g/m}^3$ (b) Case #10, $IWC = 8.7 \text{ g/m}^3$, $LWC = 3.4 \text{ g/m}^3$ (c) Case #12, $IWC = 3.8 \text{ g/m}^3$, $LWC = 3.4 \text{ g/m}^3$ 

(d) Far view of the Case #8 accreted ice shape predicted by TAICE.

Figure 11: Accreted ice shape comparison at $T_s = -5^\circ\text{C}$. Black line shows accreted ice after 120 s.

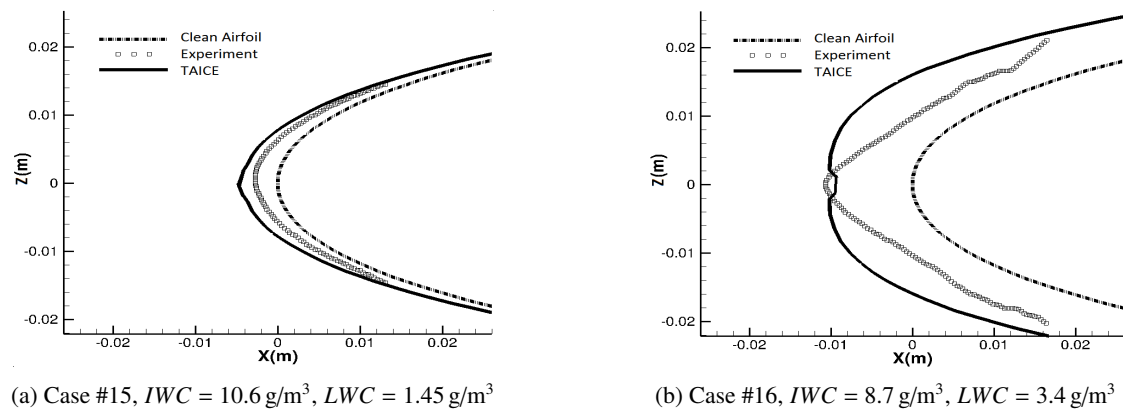


Figure 12: Accreted ice shape comparison at $T_s = -15$ °C. Black line shows accreted ice after 120 s.

5. Conclusion

Ice shape predictions are performed for various ice accretion conditions on finite wings. TUBS and COX mixed phase experimental test results are selected for the validation of the tool. Extended Messinger Model, which is further modified for mixed phase icing problems, have been used. Moreover, the models which are implemented during the HAIC project for ice crystal accretion are utilized in this study as well. Corresponding analyses have been performed with the same calibration parameters which are defined in the validation study of the 2-D version of the tool. The droplet and crystal trajectories have been calculated using a parallel computing approach, which significantly reduces the run time since almost 99 % of all computational time is spent for the particle trajectories. Moreover, additional analyses have been performed for evaluating the effect of panel numbers and time segments on accreted ice shapes. A relation similar to the recommended one in LEWICE manual is used for calculating required time segments and panel numbers have been optimized as discussed in the results part. Thus, the validation analyses indicate that results seem consistent with the experimental ones and the developed tool is capable of satisfactorily predicting ice shapes including mixed phase cases on aircraft wings. However, further effort is required for erosion effect modeling and calibration which is left as a future activity.

References

- [1] *Users Manual for LEWICE Version 3.2 2008*.
- [2] Notice of proposed amendment. *European Aviation Safety Agency 2011-03*, 2011.
- [3] Certification specifications and acceptable means of compliance for large aeroplanes cs-25. *European Aviation Safety Agency*, 2016.
- [4] Part-25 airworthiness standards: Transport category airplanes. *Federal Aviation Administration*, 2016.
- [5] K Al-Khalil, E Irabi, and D Miller. Mixed phase icing simulation and testing at the cox icing wind tunnel modeling in glennice with application to engine icing. *41st AIAA Aerospace Sciences Meeting and Exhibit*, (0903), 2003.
- [6] E Ayan and S Özgen. In flight ice accretion simulation in mixed phase conditions. *The Aeronautical Journal-Under Review*, 2017.
- [7] E Ayan, S Özgen, and M. Cambek. Mixed phase ice accretion prediction with taice. In *8th AIAA Atmospheric and Space Environments Conference*. AIAA 2016-3743, 2016.
- [8] E Ayan, S Özgen, and E Tarhan. Effect of drag coefficient models on ice crystal trajectories and secondary particle behavior in ice accretion prediction. In *Eighth Ankara International Aerospace Conference*, 2015.
- [9] S Bansmer and A Baumert. rom high altitude clouds to a icing wind tunnel: en route to understand ice crystal icing. 2017.

MIXED PHASE ICING WITH TAICE-3D

- [10] A Baumert, S Bansmer, S. Sattler, H Pervier, and B M Esposito. Simulating natural ice crystal cloud conditions for icing wind tunnel experiments - a review on the design, commissioning and calibration of the tu braunschweig ice crystal generation system. 2016.
- [11] A Baumert, P Trontine, S. Bansmer, and P Villedieu. Experimental and numerical investigations on aircraft icing at mixed phase icing conditions. *Progress in Aerospace Sciences (to be published)*, 2017.
- [12] A Hölzer and M Sommerfeld. New simple correlation formula for the drag coefficient of non-spherical particles. *Powder Technology*, 184:361–365, 2008.
- [13] T G Myers. Extension the messinger model for aircraft icing. *AIAA J.*, 2(39):211–218, 2001.
- [14] S Özgen and M Canbek. In-flight ice formationsimulation on finite wings and air intakes. *The Aeronautical J.*, 116(1178):337–362, 2012.
- [15] P Trontin, G Blanchard, and P Villedieu. A comprehensive numerical model for mixed-phase and glaciated icing conditions. In *8th AIAA Atmospheric and Space Environments Conference*. AIAA 2016-3742, 2016.
- [16] W B Wright, P C E Jorgenson, and J P Veres. Mixed phase modeling in glennice with application to engine icing. In *AIAA Guidance, Navigation, and Control Conference*, 2010.